A Prototype High-Intensity Infrasonic Test Chamber (HILF 1)

H. Edwin Boesch, Jr., and Christian G. Reiff
U.S. Army Research Laboratory
Adelphi, MD 20783

Bruce T. Benwell
Directed Energy Technologies
Sumerduck VA 22742

Abstract

We describe the conception, design, mathematical modeling, construction, and test of a prototype acoustic test chamber intended to support the performance of high-intensity acoustic target effects experiments on large targets at infrasonic and low sonic frequencies. In a series of experiments, the initial design for the test chamber system (high-intensity low-frequency 1: HILF1) produced continuous sinusoidal sound pressure levels in excess of 140 dB over a frequency range of 5 to 20 Hz within a test volume of 5 m^3.

1. Introduction

For several years, the Department of Defense Joint Non-lethal Weapons Directorate, through the Close Combat Armaments Center at Tank-Automotive and Armaments Command/Armament Research, Development and Engineering Center (TACOM/ARDEC) has sponsored an effort—the Nonlethal Acoustic Weapons (NLAWs) Program--to demonstrate acoustic technologies that may be useful for nonlethal weapons. The U.S. Army Research Laboratory (ARL) Nonlethal Acoustics Group has supported the NLAWs program with field and laboratory measurements, technical advice, and research into the design of high-intensity acoustic sources. Of particular interest for NLAW applications are the effects of sound at very low audible or subaudible (infrasonic) frequencies.

The generation of controllable and intense infrasound is a difficult problem. The very large wavelengths involved render most sources of high-intensity sound (such as loudspeakers, sirens, or horn-coupled flow modulators) inefficient or completely ineffective at frequencies below a few tens of Hertz.

2. Proposed Acoustic Test Chamber

In May 1998, the ARL acoustics team in consultation with ARDEC staff addressed the problem of designing an acoustic test facility for acoustic effects experiments. This conceptual facility would consist of a test chamber and an associated source of acoustic energy. The goals for the test facility design included (1) a test volume sufficient to hold test items and associated experimental apparatus (about 5 m^3), (2) a frequency range capability from the lower audible range (about 20 Hz) down to the single-digit infrasonic range (about 5 Hz), and (3) a uniform sound field in the chamber with an accurately controllable intensity up to 160 dB.

The starting point for our design was some form of closed chamber driven by acoustic energy from a flow modulator and a compressed air source. A flow modulator is, in essence, a valve that creates acoustic energy from a continuous airflow by varying that flow with an aperture

controlled by an electrical signal. As opposed to loudspeaker sources that are limited to acoustic intensities near 140 dB, flow modulators are capable of intensities limited only by the available air pressure and atmospheric nonlinearities. As a matter of necessity (to limit the exposure of personnel to high-intensity sound) and convenience (a controlled, accessible, and weather-independent environment), acoustic effects experiments generally employ closed exposure chambers. In addition, closed chambers make possible the concentration of the acoustic energy in a small volume and offer the potential of increased acoustic intensities from sources of limited power. Use of a closed chamber also makes possible the amplification of acoustic intensities by tuning the chamber to resonate at the desired frequency.

There are two types of resonant acoustic chambers: resonance tubes and Helmholtz resonators. The former operate at wavelengths no greater than half their major dimension: to operate at 10 Hz, a chamber would have to be at least 16 m long. In addition, resonance tubes by nature produce a highly nonuniform sound field (standing wave). On the other hand, Helmholtz resonators operate at wavelengths greater than their largest dimensions and produce uniform sound fields throughout the resonant volume. We decided that the ideal *infrasonic* test chamber would take advantage of the high gain present within a Helmholtz resonator yet have the frequency tunability of a ported bass reflex enclosure. The test chamber would consist of a structurally massive test chamber of moderate volume with a port vented to free space and tunable for frequency selectability. The acoustic power source to drive this chamber would be a high-flow dc air supply modulated by an airflow modulator. We anticipated that sound pressures of 160 dB over a frequency range from 3 to 20 Hz would be achievable. Figure 1 shows a diagram of our initial design for the high-intensity low-frequency (HILF1) test chamber system.

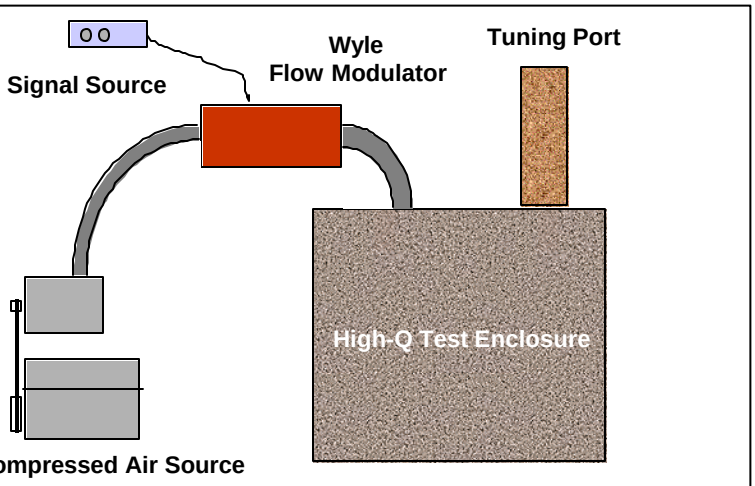

Figure 1. Diagram of proposed infrasonic test chamber.

3. Theoretical Response of Test Chamber

To evaluate the feasibility of this ported test chamber-Helmholtz resonator, we modeled the overall system taking advantage of the fact that, since we were working at infrasonic frequencies, the dimensions of the chamber and ports are necessarily small compared to the acoustic wavelength. This wavelength-to-chamber-dimension relationship allowed for a significant simplification in modeling the response of the chamber since acoustic lumped elements could be used to represent the reactive (energy storage) and loss (dissipation) elements. Standard circuit analysis techniques could then be employed to theoretically predict the frequency response and sound pressure level (SPL) within the chamber.

Figure 2 shows the electrical circuit used to model the response of the source, chamber and ports. In this model, loss elements (port radiation, viscous losses within the port, and wall absorption losses) are modeled as resistors. Air-mass displacement terms are modeled as inductors, and the compressed air volume within the chamber is modeled as an acoustic compliance or capacitance. The magnitude of the acoustic intensity inside the chamber is simply the voltage across the chamber compliance/capacitor C_{ac}. The magnitudes of the following circuit elements were derived either by hand or from Beranek [2] or Seto [3].

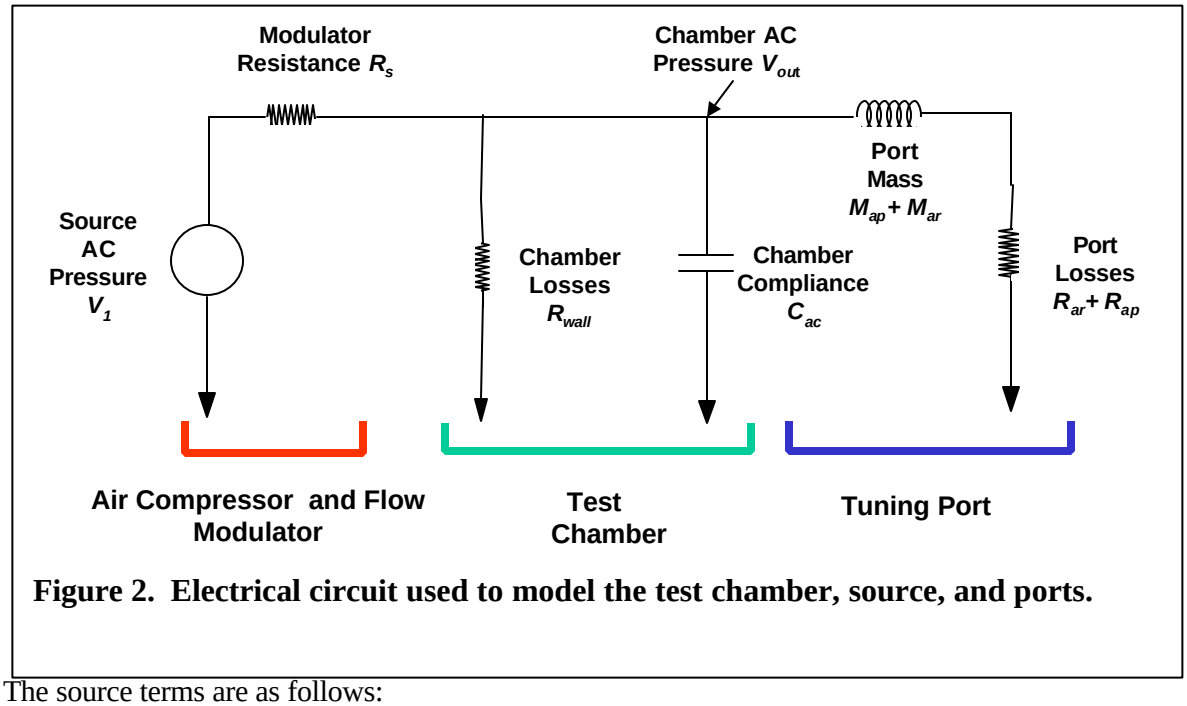

Figure 2. Electrical circuit used to model the test chamber, source, and ports.

The source terms are as follows:

R_s (equivalent source resistance) = P_1/v , [Pa/(m^3/sec)] (1)

where: P_1 = source pressure in Pascals (Pa) and

v = volume velocity in m^3/sec.

The chamber terms are as follows:

C_{ac} (chamber compliance) = $V/(r\ c^2)$, [m^5/N] (2)

where: V = chamber volume,

r = density, and

c = speed of sound.

$R_{\text{wall}} = (2\gamma Po)/(c\ C_{abs}\ S)$, (3)

where: γ = specific heat = 1.4,

P_o = atmospheric pressure in Pa,

C_{abs} = wall absorption coefficient , and

S = wall surface area.

The port terms seen by the chamber are as follows:

M_{ap} (mass of air in port) = $(L + 0.6\,a_2)\,r\,/(p\,a_2^{\,2})$, [kg/m^4] (4)

where: a_2 = radius of port and

L = port length.

R_{ap} (viscous losses in port) = $(1/(p\,a_2^{\,2}))\,r\,(2\ w\ m)^{1/2}\ [(L/a_2) + 1]$ (5)

where: $w = 2\,p\,f$,

m = kinetic coefficient of friction = 1.56E-5 m^2/sec at 20 ºC and 0.76 mm Hg, and f = frequency.

The port terms exterior to the chamber are as follows:

M_{ar} (acoustic mass of front side of port) = $0.23/a_2$. [kg/m^4] (6)

R_{ar} (radiation resistance) = $(\rho f^2 r) / c$. (7)

The circuit shown in Figure 2 can be thought of as a simple parallel *RLC* circuit. Solving the circuit equations with the actual component values shows that the circuit response is underdamped and, further, that the circuit forced response simplifies to a single exponential function with a damping factor α equal to $\frac{1}{2} R_{eff} C_{ac}$, where R_{eff} is the effective loss term from all the chamber and port losses. The natural resonant frequency of the chamber and port combination (in radians) is

$$\omega_d = (\omega_o^2 - \alpha^2)^{1/2}, \quad (8)$$

where $\omega_0 = 1/ (M_{eff} C_{eq})^{1/2}$ and M_{eff} is the effective total acoustic mass of the port (both internal and external terms)

.

A typical theoretical response for the circuit is shown by the upper smooth dotted curve in Figure 3. For this case, the chamber consists of a 5 x 5 x 6.75 ft tank with a 23-in. diam port 4.5 in. long that is driven by a modulated dc air supply of 6 psig (peak) at 1200 cfm. The major feature of the response is the peak at the natural resonant frequency, ω_d. This resonant frequency is determined by the reactive components in the circuit. Since the chamber volume C_{ac} is fixed, varying the length and, therefore, the inductance of the port adjusts the resonant frequency. Table 1 summarizes the amplitude and resonant frequencies to be expected from a 5 x 5 x 6.75 ft concrete chamber for some typical port dimensions. Also shown in the table is the half-power bandwidth and corresponding *Q* for the chamber determined from the width of the resonance in the calculated circuit response. *Q* is a measure of the ability of the chamber to *store* acoustic energy; it is the ratio of the energy density in the chamber to the energy lost per cycle at the resonant frequency. *Q* is affected directly by the chamber and port loss terms, since these terms represent the mechanisms by which acoustic power is lost from the system.

Port shape	Size (in.)	Length (in.)	Resonant frequency (Hz)	Peak amplitude (dB)	Half-power bandwidth (Hz)/ *Q*
Circular	23	4.5	18.1	153.1	0.9/20.1
Square	12	30	7.6	155.7	0.5/15.2
Square	12	54	5.9	157.2	0.5/11.8

Table 1. Predicted response of a 5 x 5 x 6.75 ft concrete test chamber when excited by a modulated dc airflow at 6 psig (peak) and 1200 cfm.

Here, we summarize some of the trends predicted by the model:

1. The resonant frequency is inversely related to the square of the chamber volume (smaller volumes generate higher resonant frequencies).
2. The resonant frequency is proportional to the square of the port area (larger port areas generate higher resonant frequencies).

3. The resonant frequency is inversely proportional to the square of the port length (larger port lengths generate lower resonant frequencies).
4. The acoustic intensity in the chamber is maximized by minimizing the equivalent modulator impedance (the source should produce a high flow at low pressure with minimal restriction in the modulator).

Our first attempt at validating our lumped circuit model was to compare our predictions

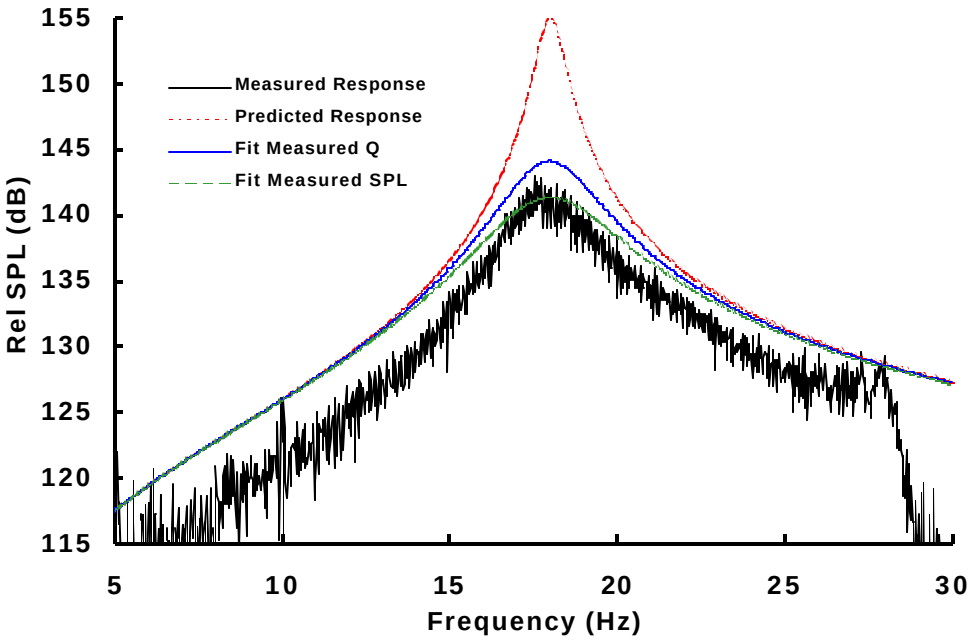

Figure 3. Predicted and measured response of prototype test chamber with 23-in. diam by 4-in. long port attached. Upper dotted smooth curve is predicted response based on electrical analog model in figure 2. Jagged solid curve is actual measured response of chamber. Other curves are model response calculations altered to fit measured response.

to the theoretical response predicted using an ANSYS physics software model [4]. The ANSYS model provided an excellent unbiased comparison since ANSYS is a finite element modeling package for solving the acoustic wave equations and did not use the lumped circuit models for the chamber elements derived for our calculations. Figure 4 shows the ANSYS prediction for the sound pressure in the 5 x 5 x 6.75 ft chamber and 23 in. diam port combination discussed above (see fig. 3 and table 1) when this chamber is driven by an acoustic signal at 17.86 Hz. The resonant frequency predicted by the ANSYS model is in excellent agreement with our lumped circuit model and provides independent validation of the reactive elements in that model. As expected, the figure also shows that the predicted SPL inside the chamber is nearly uniform at resonance. Unfortunately, the ANSYS model cannot accurately treat either the acoustic energy source or its coupling to the chamber or the loss elements in the model and, therefore, cannot accurately estimate the absolute intensity.

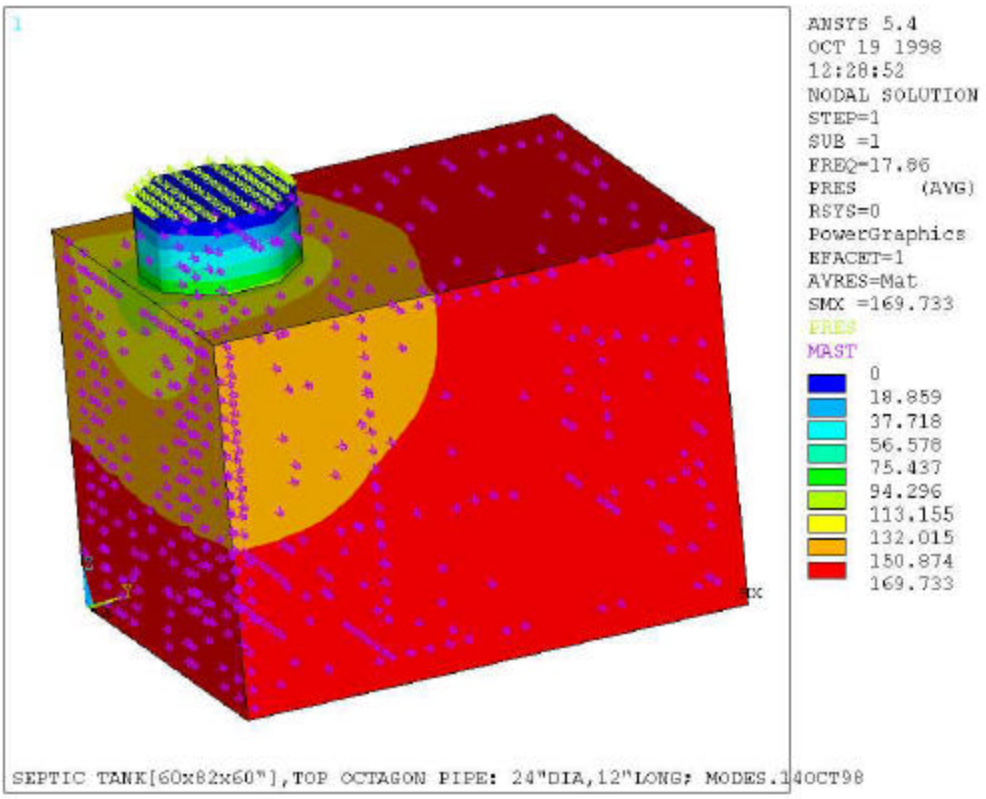

Figure 4. ANSYS finite-difference calculation for sound pressure at 17.86 Hz in prototype test chamber with 23-in. diam by 4-in. long port.

4. Analysis of Chamber Wall Losses

The equation that defines R_{wall} (shown in section 3) is based on the acoustic absorption (or absorption coefficient), C_{abs}, of the inner wall surfaces. The absorption coefficient is simply an effective measure of the fraction of acoustic energy incident on a surface that is not absorbed by that surface (i.e., $C_{abs} = 0.1$ means 10% absorption). The absorption coefficient generally decreases with decreasing frequency.

The absorption coefficient used for our model was based on data measured for unpainted concrete walls measured over a frequency range from 128 to 4096 Hz [3]. A frequency-dependent equation was then derived to extrapolate these data to the frequencies of interest to our investigation (<20Hz). Figure 5 shows the experimentally derived absorption coefficients from [4] as well as the extrapolated curve used to determine the value of R_{wall} at lower frequencies. This figure shows that extrapolated absorption coefficients are 0.35%, 0.39%, and 0.56 % at 5.8, 7.4, and 18.0 Hz respectively. It was these extrapolated coefficients that were used to calculate the value of R_{wall} in the theoretical model used to predict the SPL within the chamber.

It is important to stress that at very low frequencies, wall absorption is not necessarily the dominant loss term for a structure. At large wavelengths, the wall's structural integrity, rigidity, or stiffness cannot be ignored and the work that goes into wall displacement (flexure) or vibration will dominate. The loss factor associated with wall integrity cannot be easily defined since it is uniquely dependent on the individual wall and fabrication process. Various references indicate

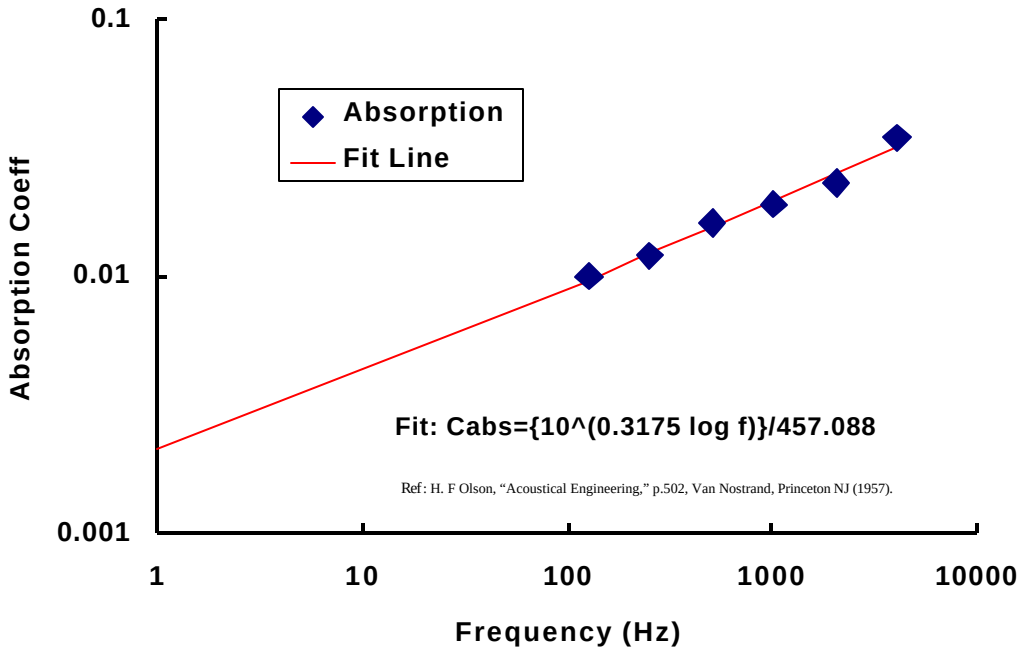

Figure 5. Experimentally derived and extrapolated absorption coefficients used to determine value of R_{wall}.

that well-made (structurally rigid) enclosures exhibit a wall absorption that decreases with frequency (see fig. 5), with one exception. At low frequencies (a frequency value that cannot be easily predicted since it is unique to the structure in question) the coefficient flattens out to a constant value typically no less than approximately 1%. The frequency at which the coefficient tends to become constant is typically between 10 and 30 Hertz.

5. Construction of Prototype Test Chamber

To validate the circuit model that we derived for the proposed test chamber, we constructed and then tested an experimental prototype. The ideal test chamber for these tests would be both infinitely massive and stiff to eliminate wall-absorption and vibration losses at these extremely low frequencies. Since the ideal chamber is not achievable, we decided to use a precast concrete chamber in hopes that we could minimize wall absorption while at the same time provide enough structural integrity to minimize vibration losses. The chamber size (5 x 5 x 6.75 ft) was chosen as a compromise between the need to minimize the chamber size to maximize the resonant frequency yet maintain a large enough test volume to accommodate larger test subjects.

The chamber is actually a commercially available 1000-gal grease trap, where the floor and four walls are tied together with No.3 steel reinforcing rods spaced 12 in. on center and then pre-cast at one time with concrete. The lid includes two 23-in. diam manhole ports. For the experimental tests, one access port was used to plumb in the air source while the second access port was used to attach the tuning ports.

Two interchangeable 12-in. square tuning ports were constructed from ¾ in. exterior grade plywood and reinforced in the corners with 2 x 3-in. battens. In use, these tuning ports were mounted to one of the chamber manholes with an adapter with a 12-in. square hole and an attached 6-in. long tuning port. A skirt on one end of the longer tuning ports would slip over the 6-in.n long port on the adapter, resulting in tuning ports with total lengths of 30 in. and 54 in. The flow modulator was mounted on the inlet manhole with another adapter.

The air source used to excite the chamber consisted of the dc air supply and air flow modulator from ARL's Mobile Acoustic Source (MOAS). The dc air supply is generated with a compressor driven by a diesel engine that maintains a preset constant air pressure at the input to the flow modulator. The airflow modulator is a Wyle Laboratories model WAS 3000. In essence, this modulator is a valve with an aperture that can be varied linearly about the 50% open position by the application of electrical waveforms with frequencies up to 300 Hz. The MOAS air source and Wyle modulator could be operated at pressures from 2.7 to 15.0 psig and corresponding dc air flow rates from 820 to 1890 cfm.

Figure 6 shows the concrete test chamber, ports, and MOAS source used during the experiments. The flow modulator can be seen attached to the lid of the chamber towards the back. A 30-in. port is attached to the chamber lid near the front. Immediately in front of the chamber on the ground is a 12-in. square x 4-ft long port. The dc air compressor sits on the flatbed trailer behind the chamber but is outside the frame of the picture. Figure 7 shows a top view of the chamber lid with the Wyle modulator at the right mounted on its cradle and adapter (note the 4-in. diam air hose from the MOAS compressed air source) and the 30-in. long tuning port installed on the adapter at the left.

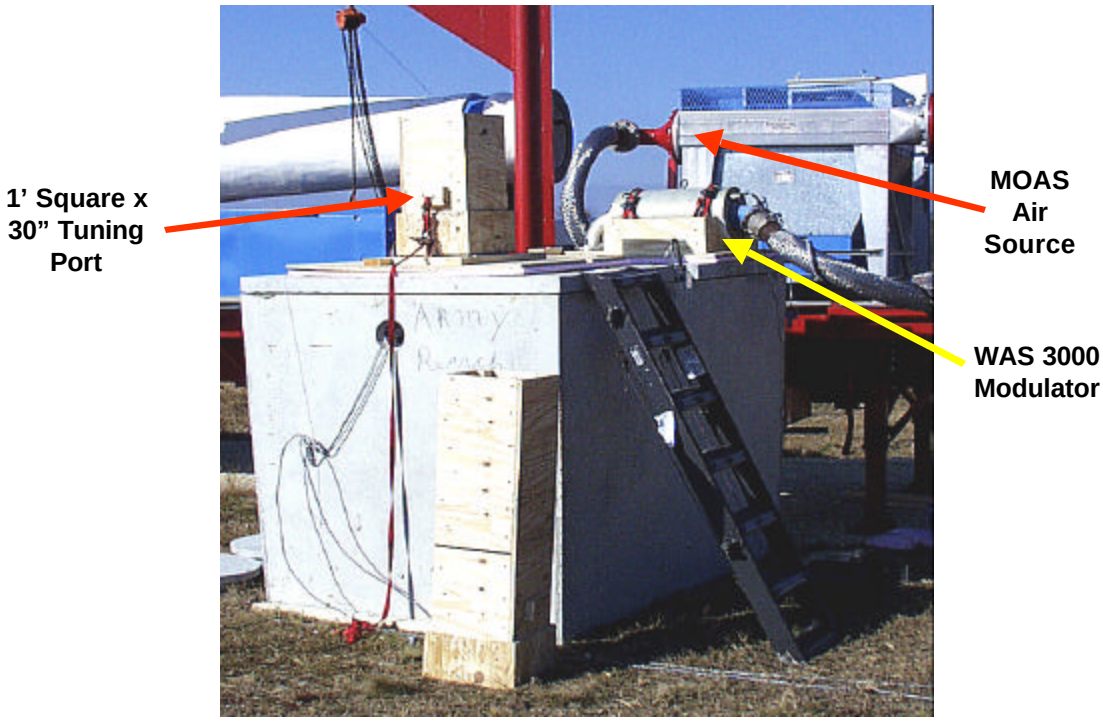

Figure 6. Concrete test chamber, ports, and MOAS source used during experiments.

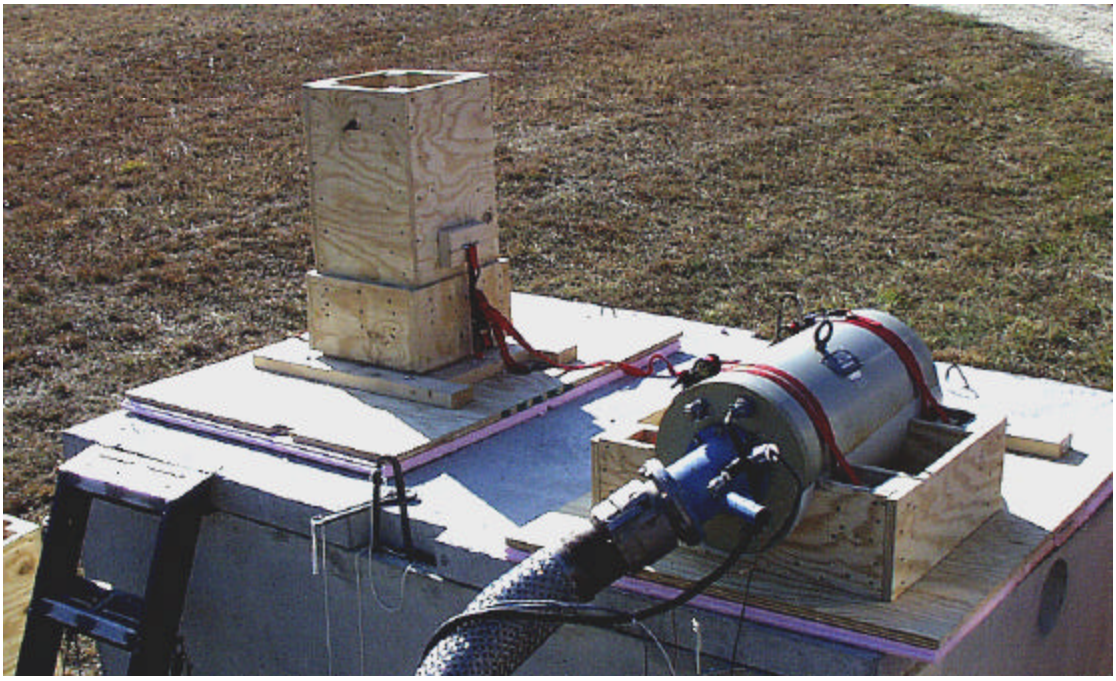

Figure 7. Detail of test chamber showing 12-in. square, 30-in. long port and MOAS modulator source mounted at access hatch openings.

6. Characterization of the Chamber

To characterize the chamber, four measurements were recorded in parallel on a digital audio tape (DAT) recorder, a digital oscilloscope, and a waveform digitizer attached to a laptop computer: Channel 1 monitored the instantaneous air pressure supplied to the modulator using a pressure transducer. Channel 2 monitored the pressure in the chamber using a microphone and preamplifier that were centered in the chamber 2 ft 6 in. from the floor and walls and 2 ft 8 in. from the end wall. (In the initial chamber response measurements, two microphones were in the chamber 2 ft 6 in. from the floor and 2 ft from each end wall.) Channels 3 and 4 monitored accelerometers attached to the ceiling and long side wall of the chamber, respectively. The sensors were mounted inside the chamber near the center and perpendicular to the surface being monitored.

6.1 Initial Chamber Response Experiment

We performed three experiments using the concrete chamber. The first experiment explored the acoustic response of the unmodified chamber driven by the MOAS modulator with each of the various tuning ports and was intended to demonstrate proof of principle and verify the design model, including the theoretical lumped circuit model and the derivations for the individual circuit elements.

Figure 3 shows the measured frequency response of the sound pressure inside the chamber with the 23-in. diam, 54-in. long port in use (ragged solid curve). The chamber was driven by a sine wave from the modulator swept from 5 to 50 Hz with 6 psig input pressure. The observed resonant peak is at 18.3 Hz. This is within 2% of the calculated frequency of 18.0 Hz (solid smooth curve in figure). Near resonance, the chamber is uniformly filled (within 1 dB as

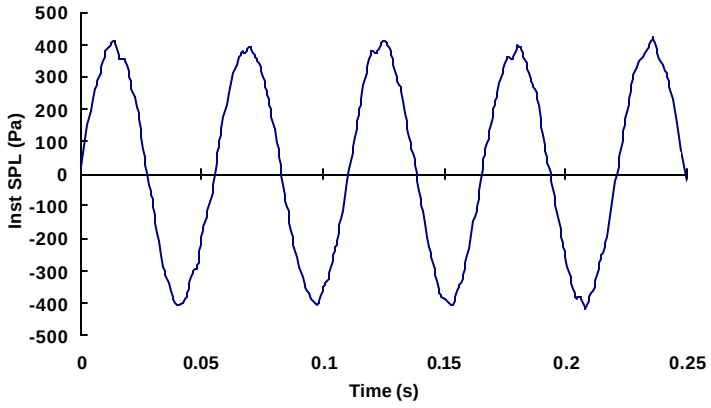

Figure 8. Waveform of acoustic signal in chamber with 23-in. diameter by 4-in. long port attached and using 18 Hz excitation.

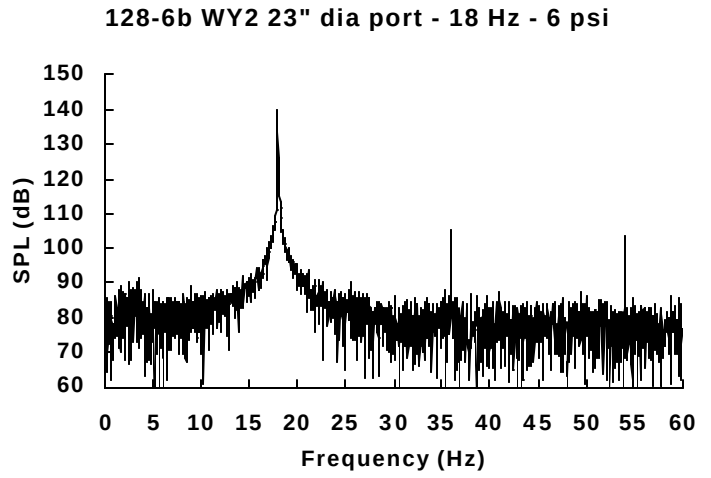

Figure 9. Spectrum of acoustic signal in chamber with 23-in. diameter by 4-in. long port attached and using 18 Hz excitation.

measured approx. 2 ft above the floor) with a very pure acoustic sine wave; the waveform at 18.0 Hz is shown in figure 8. The spectral content of this waveform as obtained by fast Fourier transform (FFT) analysis is shown in figure 9**.** The second and third harmonics are more than 35 dB below the intensity of the fundamental at 18 Hz. At 18.3 Hz, 99.8% of the total acoustic energy is at the resonant frequency. Unfortunately, comparison of the measured and predicted response in figure 3 shows that the intensity of the measured sound pressure at resonance is approximately 15 dB less than anticipated. Also, in comparison to the initially predicted response, the measured response also shows a much wider peak at resonance, corresponding to a substantially larger bandwidth and a lower *Q* for the system than we predicted. Figures 10 and 11 show results for equivalent tests using the 12 in. square, 54-in. long port and 6 psig input pressure to the modulator. Here, the observed resonance is at 5.8 Hz (ragged solid curve in fig. 10); again, this is within the measurement error of the calculated resonant frequency. The FFT of the acoustic signal recorded at 5.8 Hz (fig.11) confirms the purity of the waveform at resonance in the chamber. Again, we can observe in fig.10 that the measured intensity in the chamber at resonance is over 15 dB below the initially predicted level and that the measured bandwith is greater than expected (*Q* is less than expected). Table 2 summarizes the results of these tests. The data from tables 1 and 2 are compared in figures 12 to 14. Figure 12 compares the predicted and measured resonant frequencies. This figure shows that the measured resonant frequencies are in almost exact agreement (within 2%) with the predicted value. This validates the derivation of each of the reactive elements in the model. However, as we have noted, figure 13 shows that the SPL measured for each port configuration is about 15 dB less than expected. Figure 14 shows that in each case the half-power bandwidth at resonance is substantially greater than expected.

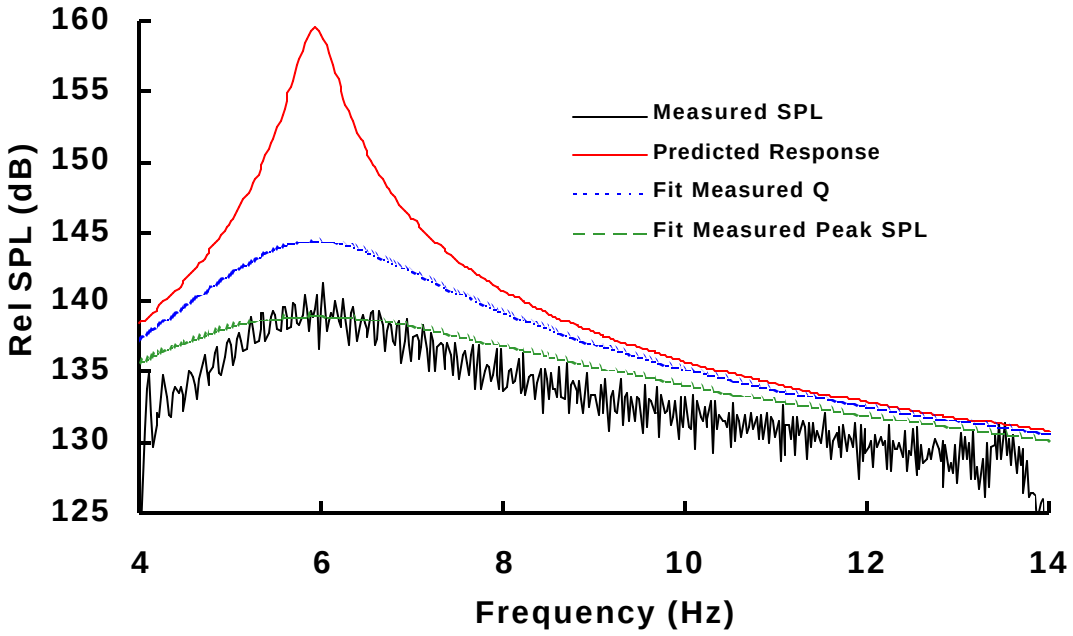

Figure 10. Predicted and measured response of prototype test chamber with 12-in. square by 54-in. long port attached. Upper smooth curve is predicted response based on electrical analog model in figure 2. Jagged solid curve is actual measured response of chamber. Other curves are model response calculations altered to fit measured response.

The discrepancies between the predicted and observed peak acoustic intensities and predicted and observed system bandwidths indicate that the system contains losses that we did not include in the initial model. In our model, increased chamber losses correspond to a reduced value for the parallel loss resistance (fig. 2). The dotted smooth curves in figures 3 and 10 correspond to system responses calculated with chamber losses adjusted to match the bandwidth (or Q) of the measured response. This adjustment also brings the modeled intensity at resonance into closer agreement with the observations. Thus, based on the experiments performed on the concrete test chamber, we can infer from the measured data that the actual equivalent absorption coefficients for the concrete chamber were 2.1%, 1.9%, and 2.2% at 5.8, 7.4, and 18.0 Hz respectively. These measured values are substantially (4 to 6 times) larger than our extrapolated values. When the experimentally derived absorption factors are incorporated back into our chamber circuit model (in effect we modified the theoretical half-power bandwidth or system Q to match the measured data), the comparison between the measured and predicted SPL is improved by nearly 10 dB (see fig. 15). The model still overestimates the intensity by up to 5 dB (at 5.8 Hz). To match the observed intensities at resonance, the loss term C_{abs} in the model was increased (which leads to R_{loss} being reduced) still more (the lowest, dashed smooth curves in figs. 3 and 10). However, these curves are now too broad; i.e., they no longer fit the observed system bandwidth or Q. Evidently, the present model does not include some additional losses in the system that are not associated with the chamber; such losses would not affect the system Q. These losses may be associated with the modulator or with coupling of the acoustic signal into the chamber.

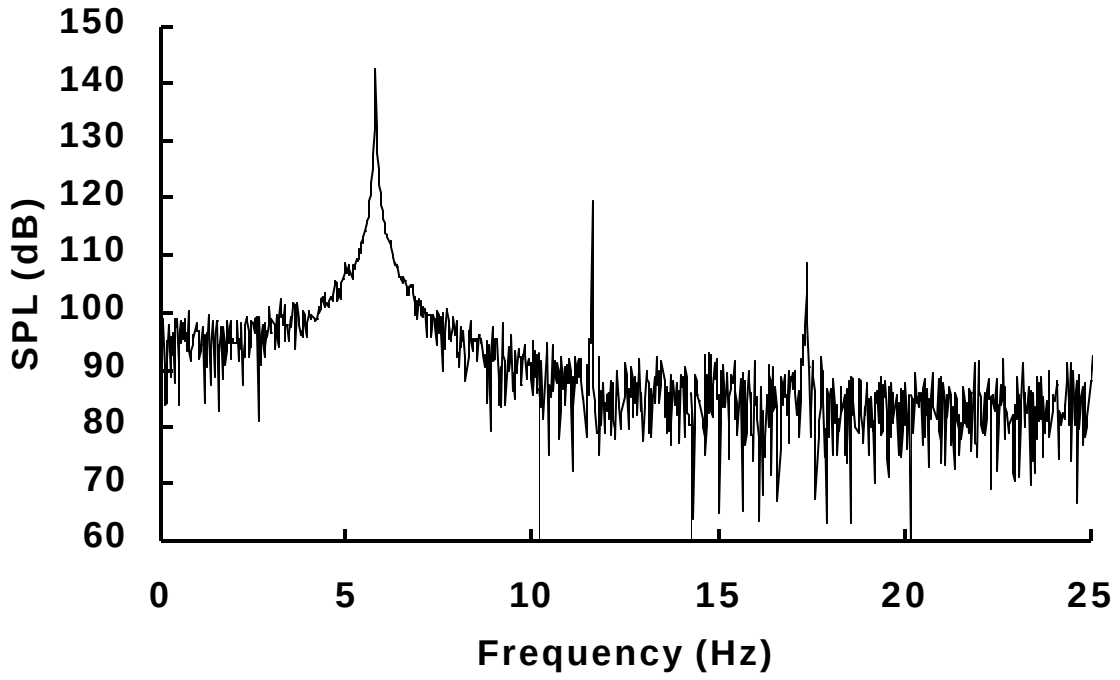

Figure 12. Spectrum of acoustic signal in chamber with 12-in. square by 54-in. long port attached and using 5.8 Hz excitation.

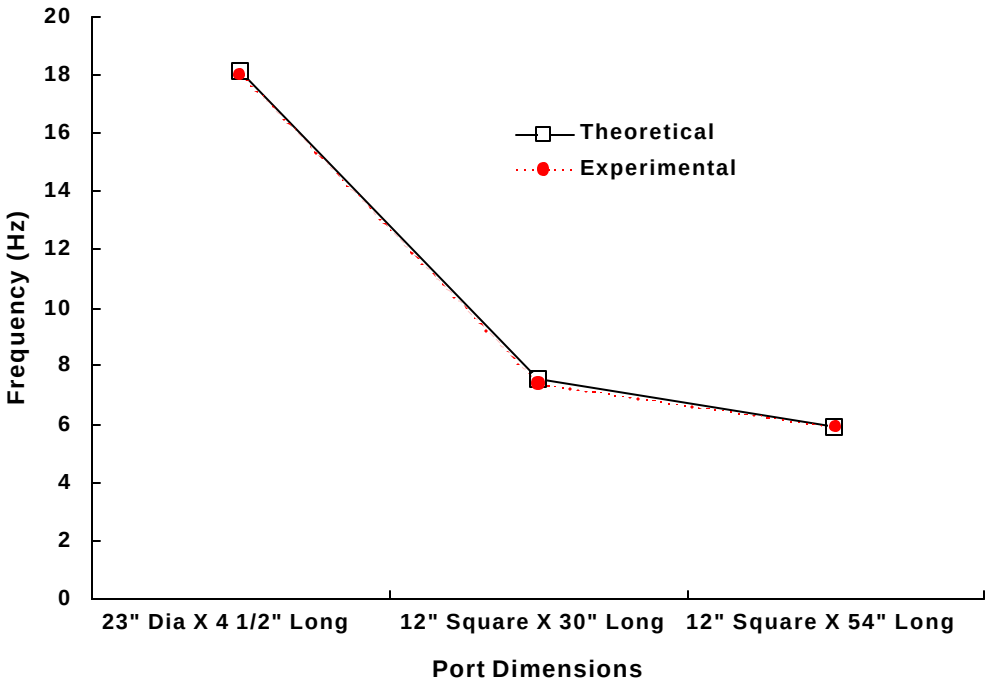

Figure 11. Comparison of predicted and measured natural resonant frequency of acoustic test chamber for various port configurations.

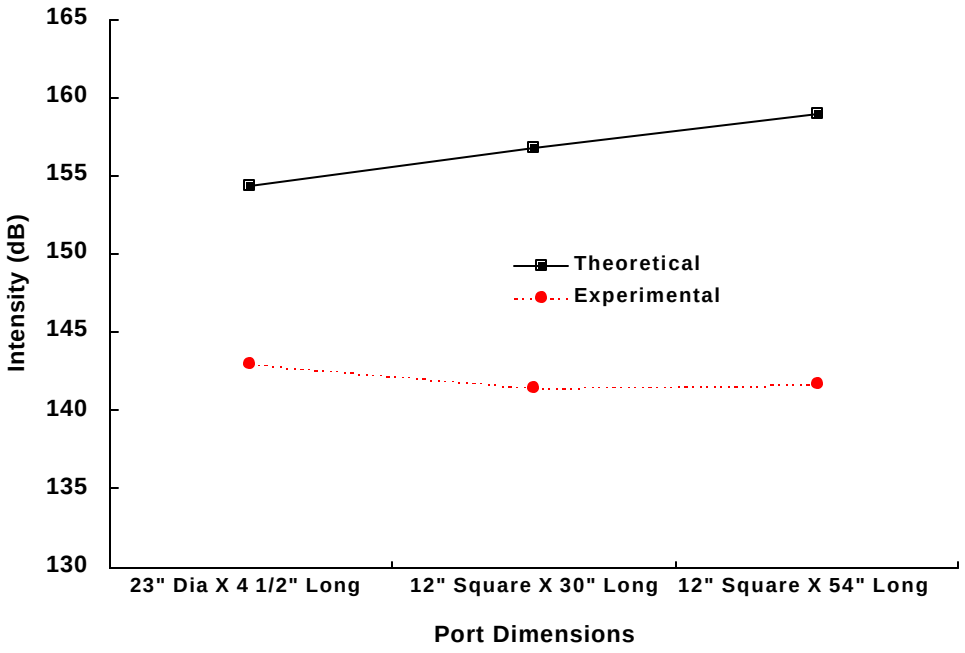

Figure 14. Comparison of predicted and measured sound pressure level inside test chamber for various port configurations.

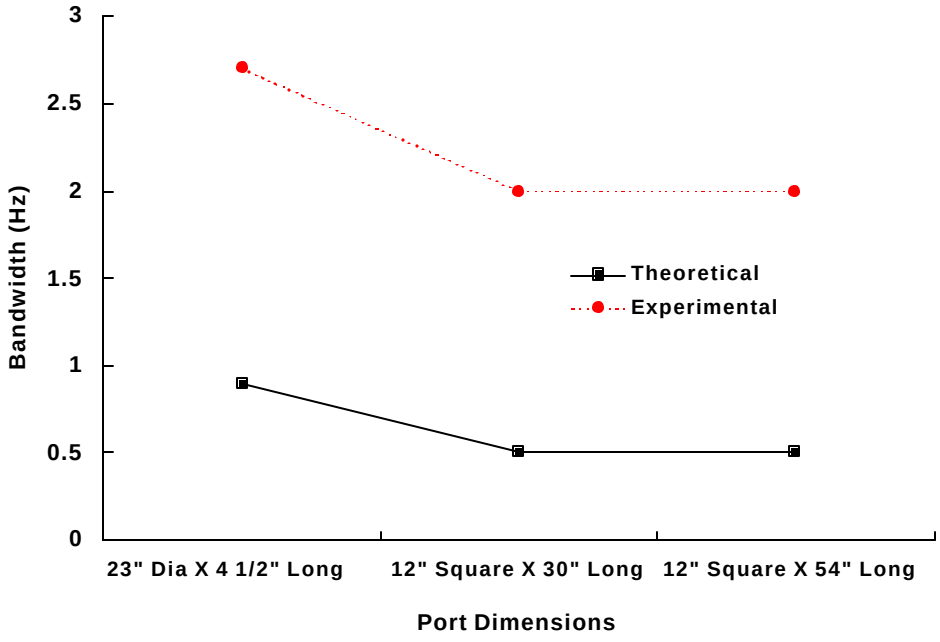

Figure 13. Comparison of predicted and measured half-power bandwidth at resonance for various port configurations.

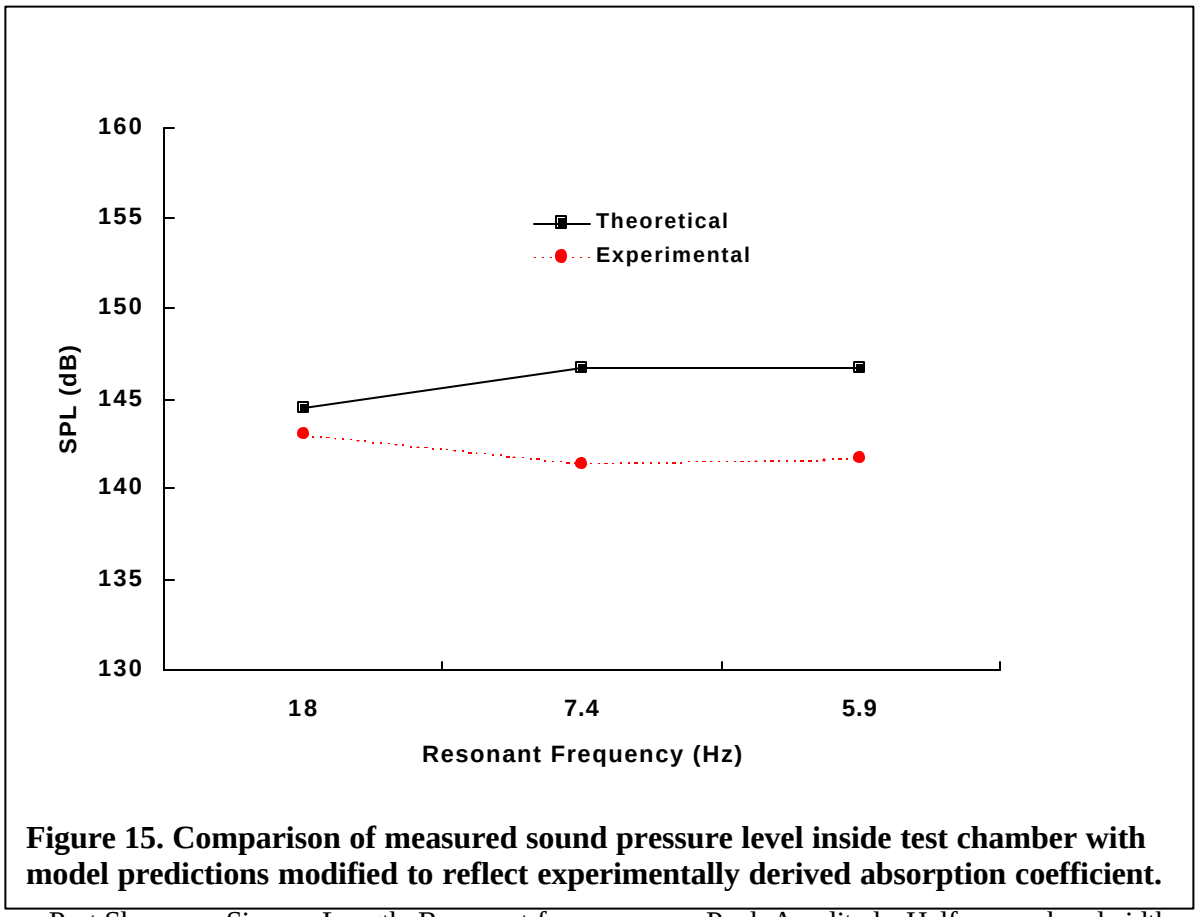

Figure 15. Comparison of measured sound pressure level inside test chamber with model predictions modified to reflect experimentally derived absorption coefficient.

Port Shape	Size (in.)	Length (in.)	Resonant frequency (Hz)	Peak Amplitude (dB)	Half-power bandwidth (Hz)
Circular	23	4.5	18	143	2.7 (6.7)
Square	12	30	7.4	141.4	1.8 (4.1)
Square	12	54	5.9	141.7	2 (2.95)

Table 2. Measured response for the 5 x 5 x 6.75 ft prototype concrete test chamber when excited by a modulated dc air flow at 6 psig nominal and 1200 cfm.

Our modeling suggests that the majority of the additional losses are accounted for by the observed change in system Q and are, therefore, attributable to the chamber. This additional chamber loss can occur as either a radiation loss from the port (R_{ar}), viscous loss through the port (R_{ap}), or losses associated with the chamber walls (R_{wall}). Because of the overall geometry of the port and chamber and the associated wavelength, it is very unlikely that there would be significant additional losses associated with either viscous and radiation losses other than what the model predicts. These loss values would need to be increased by orders of magnitude to account for the measured response of the chamber (which is geometrically unfeasible). Following the first experiment, we hypothesized that the most likely source for the additional loss was absorption or transmission of energy by the chamber walls (see section 6.2).

An additional chamber loss term not accounted for in the model may result from the dc airflow from the modulator literally blowing energy out the port. At resonance, the chamber and

port exchange acoustic energy in the form of the potential energy of air compression in the chamber and kinetic energy in the motion of the air mass in the port. If sound-induced kinetic energy in the port air mass is blown out of the port by the dc airflow such that it cannot react back on the chamber, that energy is lost to the system. Additional experiments described in section 6.3 detail a set of measurements to investigate this possible effect.

6.2 Chamber Wall-Stiffening Experiment

The actual absorption coefficient that we inferred from the initial chamber response experiment suggests that the coefficient for this chamber tended toward a constant value of approximately 2 to 3% as opposed to a frequency-dependent loss of less than 1% as extrapolated from the literature (see fig. 5). This fact lends support to our hypothesis that the additional loss we measured is due to the structural integrity of the chamber. With this in mind, in a second set of experiments we attempted to increase the rigidity of the chamber by adding reinforcing and stiffening members. We also instrumented the chamber with accelerometers to measure deflections in the walls induced by the sound pressure.

The chamber was stiffened by the addition of heavy steel rods that tied together opposite walls to reduce symmetrical expansion and contraction (breathing mode) flexure of the chamber. The rods were installed between the larger walls by first drilling small holes through the centers of the top and bottom and larger (6 ft 9 in. x 5 ft) sides. We then installed 1-inch cold rolled steel rods between the top and bottom and larger sides with 1-ft steel plates as washers on either side of the concrete walls. An epoxy-based paint was also applied to the interior of the chamber to increase the hardness of the inner wall surface.

Accelerometers were installed on the walls and lid to determine the degree of wall flexure. These accelerometers measured the movement of the side wall and lid during the experiment. The direction of the movement measured was perpendicular to the plane of the wall or lid. The purpose of the measurements was to determine the deflection or flex in the wall and lid caused by the sound pressure on the inside of the chamber. The power dissipated in this motion could be considered a loss to the system that would result in the lowered resonance amplitude of the chamber.

To calculate an upper bound on the power dissipation associated with a surface, we multiply the pressure P, the surface area of the surface in motion A_s, the deflection of the surface d_P, and the angular frequency of the deflection f:

$$P_{\text{surface}} = P\, A_s\, d_P\, (2\pi f)/\sqrt{2}. \qquad (9)$$

The deflection of the surface is found by taking the double integral of the acceleration data with respect to time; this yields

$$d_P = a / (2\pi f)^2, \qquad (10)$$

where a is the measured peak acceleration at f. To calculate the total power dissipation associated with this deflection, we double P_{surface} to account for the opposite surface.

Table 3 lists the peak acceleration found from calculating the FFT of the data, the SPL in the chamber, and the resulting power dissipation.

Table 3. Peak measured wall acceleration at 18 Hz values and resulting calculated power loss in chamber walls.

Brace status	Inlet pressure (psi)	Wall acceleration (m/s^2)	Lid acceleration (m/s^2)	Chamber pressure (Pa)	Power dissipation (4 surfaces) (W)
Loose	6	0.0137	0.00932	319	0.28
	12	0.191	0.0519[a]	469	4.3
Tightened	2.7	0.0658	0.0664	223	1.1
	8	0.126	0.116	397	3.6
	12	0.137	0.127	480	4.9

[a]The low value may be erroneous, the FFT was unlike others measured at the same location.

The peak values in table 3 were obtained by performing FFTs on the measured data and recording the peak values of each FFT at the resonant frequency of 18 Hz.

Figure 16 shows the effect of this attempt to stiffen the chamber walls on the measured acoustic response of the chamber. The addition of the steel rods produced no detectable change in the SPL measured inside the chamber. Our conclusion from this experiment is that the added steel rods caused only minor changes in the measured wall acceleration (displacement) and no detectable effect on the chamber's acoustic absorption. In hindsight this is not a surprising result.

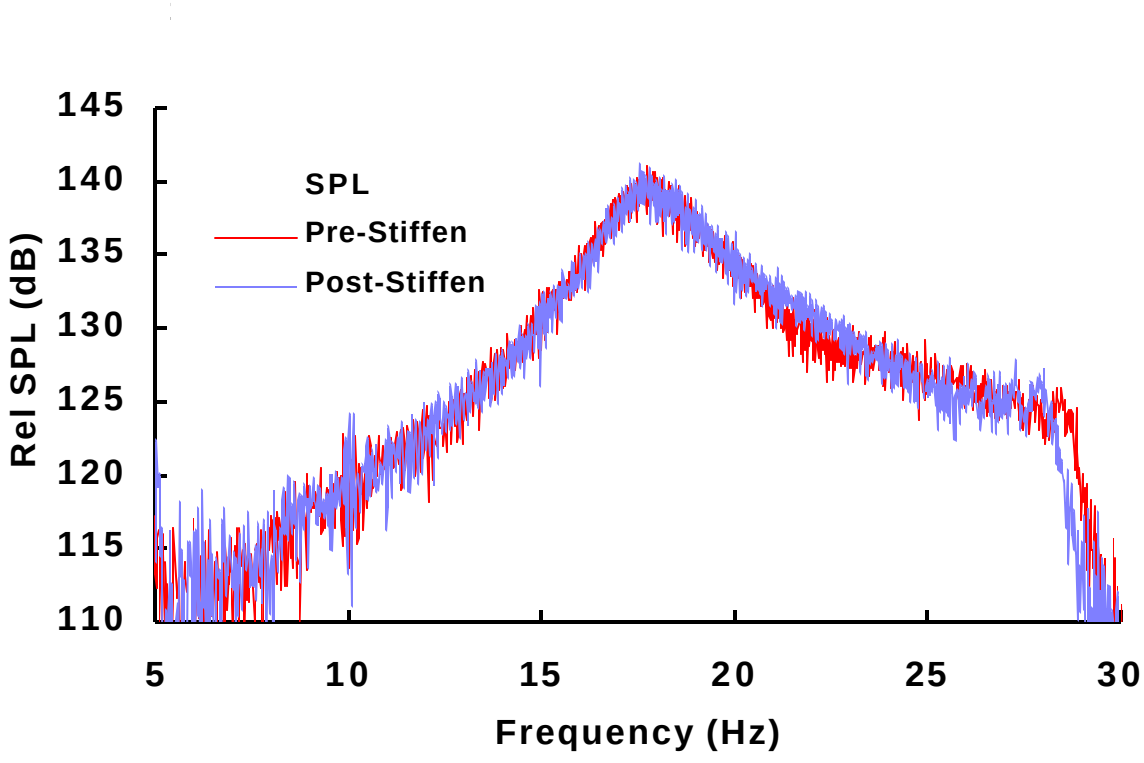

Figure 16. Comparison of measured response of the chamber with 23-in. diameter by 4-in. long port attached before and after the chamber was stiffened with steel rods.

If a well-made (structurally rigid) chamber produces absorption coefficients on the order of 1%, and we are already seeing coefficients near 2%, then we would have to make substantial structural changes to pick up an additional 1% absorption improvement.

6.3 Loudspeaker Drive Experiment

As noted in section 6, we theorized that the excess acoustic losses in the chamber might result from the dc airflow through the chamber and port associated with the operation of the air compressor-modulator acoustic source. To explore this possibility and to verify the chamber response when it is driven by a pure ac sound source (no unidirectional airflow component), we performed a third experiment with the chamber driven by a loudspeaker rather than the MOAS source and modulator. We mounted an 18-in.-diam low-frequency dynamic driver in place of the Wyle modulator at one of the hatch openings in the chamber and drove this loudspeaker with audio-frequency sweep tones from 5 to 30 Hz to record the chamber response. Figure 17 shows the measured response (ragged solid curve) of the loudspeaker-chamber system using the 23-in. diam port. Also shown in the figure is the predicted response (solid smooth curve) of the loudspeaker-driven chamber using the chamber frequency-dependent wall absorption shown in figure 5. We calculated the predicted response from an electrical analog model similar to that

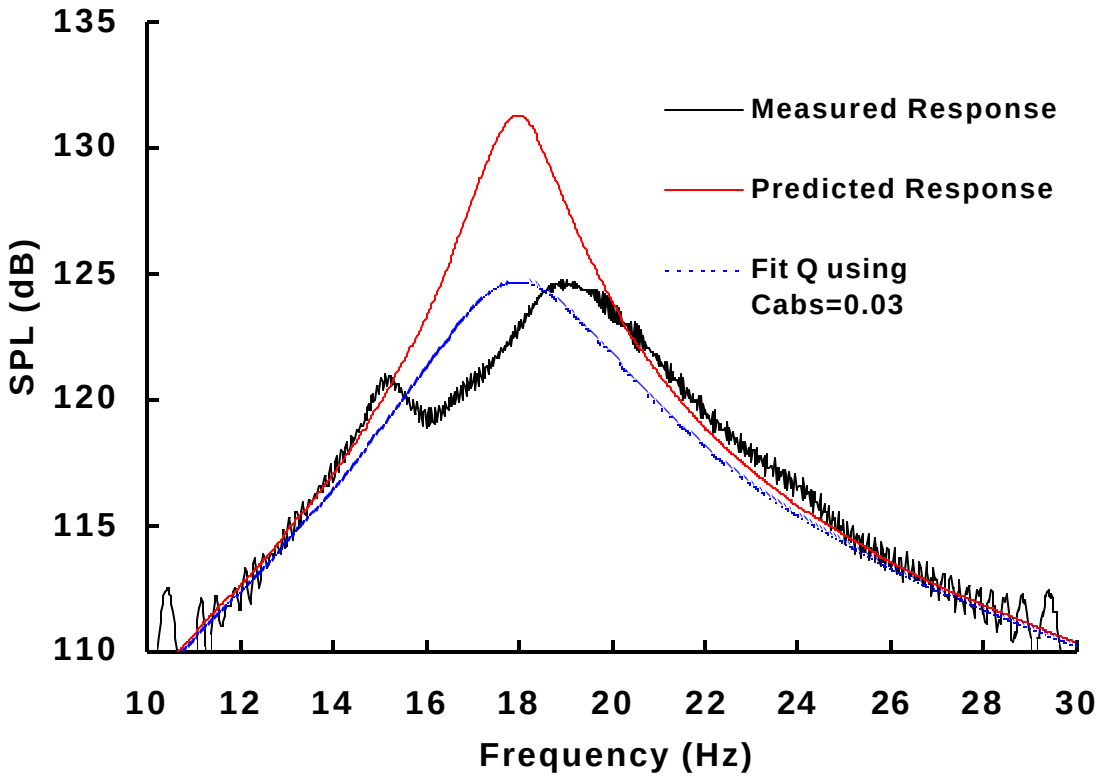

Figure 17. Measured and modeled response of the chamber with 23-in. diam by 4-in. long port excited by 18-in. loudspeaker. Jagged solid curve is measured response; smooth curves are model responses calculated using initial (upper curve) and modified (lower curve) chamber absorption.

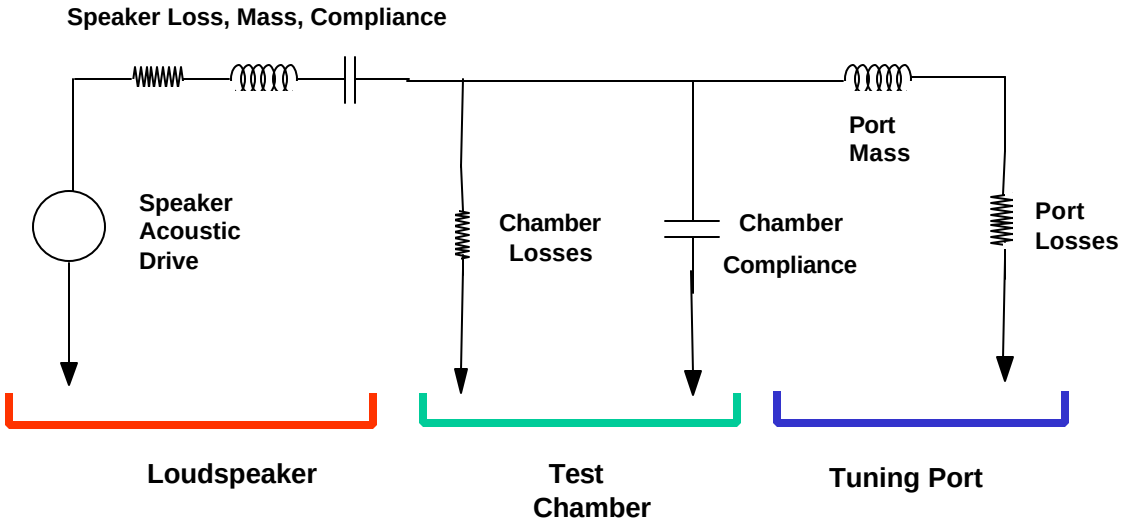

Figure 18. Electrical circuit analog of chamber driven by loudspeaker used for model calculations.

discussed in Section 3 for the modulator-driven system. A simplified schematic of this model is shown in figure 18. The loudspeaker equivalent loss, mass, and compliance were calculated from the published Thiele parameters for the model of loudspeaker used in the test [6]. Above ~10 Hz the calculated response agrees reasonably well with the observed response, with the exception of an unexplained kink in the measured response at ~16 Hz that also appears to displace the resonant peak. We also show a response curve calculated using a fixed value of 0.03 for the wall absorption coefficient; ignoring the kink, this curve is a reasonable match to the width and slope of the measured system resonant response and indicates an effective chamber *Q* of about 4.5. Therefore, the chamber *Q* and absorption measured with the loudspeaker drive are comparable to those measured with the modulator drive (table 2 and figure 3), and we conclude that the dc airflow associated with the modulator did not cause substantial additional acoustic losses under our operating conditions. This experiment also indicates that the unexpectedly high acoustic losses we observed must be associated with the chamber rather than the acoustic driver. The specific cause of these excess losses remains undetermined.

Note that, even though no attempt was made in this test to maximize the SPL in the chamber (e.g., by applying the maximum allowable drive to the loudspeaker), a respectable continuous SPL in excess of 120 dB was achieved at 18 Hz using a simple audio power amplifier-loudspeaker combination as the audio signal source. *This simplified arrangement for the test chamber may be useful for effects testing at reduced sound intensities.*

7. Further Work: Optimizing the Acoustic Intensity Within the Chamber

Our initial experiments have shown that we can develop SPLs of approximately 143 dB inside our experimental concrete test chamber driven by the MOAS source operating at its nominal conditions of 6 psig and 1200 cfm. The MOAS source is limited to a maximum pressure of 15 psig at 1890 cfm. At this level, we would induce a maximum SPL of approximately 148 dB, far less than our target SPL of >160 dB. The reason for the poor energy transfer is the substantial mismatch between the modulator impedance and the chamber impedance. The acoustic impedance of the chamber, when tuned to 18 Hz, is approximately 2 kΩ. The Wyle modulator on the other hand presents a very high impedance, over 67 kΩ, at its nominal operating parameters of 6 psig and 1200 cfm. Figure 2 shows that the large impedance mismatch between the modulator (R_s) and the chamber is in effect a substantial voltage divider between the source

and the chamber. To minimize this mismatch, the effective modulator impedance must be lowered to match the chamber impedance at resonance. *Therefore, the most promising way to extend the SPL above our 148-dB limit is to replace the WAS-3000 modulator with a modulator with a larger port area (lower acoustic impedance).* A realistic minimum-impedance modulator (largest port area) that can operate within our frequency range would present an impedance in the low kilohm range. Use of a low impedance modulator would also accommodate use of a higher-capacity air supply with its attendant greater acoustic power input to the system.

We are currently completing an improved acoustic test chamber system (HILF2) that employs a specially designed low-impedance flow modulator, a high-capacity centrifugal blower air source that theoretically has the capacity to provide 3400 cfm at 28 psig, and an improved Helmholtz resonator design. If the acoustic losses in this system prove to be no worse than those we measured in HILF1, we expect to generate SPLs inside the chamber in excess of 155 dB.

8. Conclusions

We have designed, modeled, constructed, and performed response measurements and analysis on a prototype acoustic test chamber intended to support high-intensity acoustic target effects experiments at infrasonic frequencies. The experiments and analysis presented here have successfully demonstrated our design concept and show that we can generate high-intensity infrasonic sound pressure levels over a test volume large enough to perform complex experiments on large test items. Initial tests showed that SPLs of at least 143 dB could be generated over a frequency range of 5 to 20 Hz within a test volume of 5 m^3. Modeling results indicate that further upgrades to the system (use of a high-capacity centrifugal blower air source, a specially designed low-impedance modulator, and an optimized chamber design) should allow us to extend the SPL to at least 155 dB. Finally, we note that continuous sound intensities in excess of 120 dB were easily achieved in the prototype chamber using a simple power amplifier-loudspeaker combination as the audio signal source. This simplified arrangement for the test chamber may be useful for effects testing at reduced sound intensities.

References

1.B. Benwell, D. Detroye, H. E. Boesch, Jr., and V. Ellis, *Multiple Plasma Channel High Output Variable Electro-acoustic Pulse Source*, U.S. patent No. 5,903,518 (May 1999).

2. L. L. Beranek, *Acoustics*, McGraw-Hill, New York (1954).

3. W. Seto, *Theory and Problems of Acoustics*, (1971).

4. H.F. Olson, *Acoustical Engineering*, Van Nostrand, Princeton, NJ (1957), p.502.

5. John Domen, TACOM/ARDEC, private communications (July-October 1998).

6. D. B. Weems, *Designing, Building and Testing Your Own Speaker System,* McGraw-Hill, New York (1990).